

Fragile magnetic order in metallic quasicrystals

Ronaldo N. Araújo,¹ Carlo C. Bellinati,² and Eric C. Andrade²

¹*Instituto de Física de São Carlos, Universidade de São Paulo, 13560-970, São Carlos, SP Brazil*

²*Instituto de Física, Universidade de São Paulo, 05315-970, São Paulo, SP, Brazil*

(Dated: October 17, 2024)

Inspired by recent experimental studies of local magnetic moments interacting with a metallic quasicrystal, we study the low-temperature fate of spins placed in two-dimensional tilings. In the diluted local moment limit, we calculate the spin relaxation rate $1/T_1$, as measured by electron spin resonance, and show that it displays a marked dependence on the system size N and the filling n of the electronic bath. For a finite concentration of spins, we integrate out the conduction electrons and generate an effective magnetic coupling between the local moments, which we treat as Ising spins. Despite the strongly frustrating nature of the magnetic couplings and the lack of periodicity in the problem, we find long-range orders for finite N in our large-scale Monte Carlo simulations. However, the resulting magnetically state is fragile, as clusters of essentially free spins fluctuate down to very low temperatures.

I. INTRODUCTION

Quasicrystals are ordered solids with a peculiar non-periodic arrangement of atoms: their diffraction patterns show well-defined Bragg peaks while exhibiting symmetries that are forbidden in periodic systems [1, 2]. Over the last years, platforms based on Moiré systems [3–5], optical lattices [6], and arrays of artificial atoms [7] are complementing the existing solid-state materials and opening the venues for new experimental and theoretical investigations on quasicrystals. The lack of periodicity in quasicrystals invalidates Bloch’s theorem and poses an extra challenge in understanding the effects of topology and electronic correlations in a quasiperiodic environment with both conventional and unconventional behavior reported, for instance, for topological electronic properties [8–10], local moment magnetism [11–15] and superconductivity [16–21].

One interesting question in metallic quasicrystals is the resulting ordered state of local moments placed on this system as we integrate out the conduction electrons. For its crystalline counterpart, these local moments interact via the Ruderman–Kittel–Kasuya–Yosida (RKKY) coupling [22]. Due to the underlying lattice periodicity, the local moment’s position is random, and for a moderate concentration of magnetic impurities, one typically finds a spin-glass ground state [23]. In quasicrystals, the situation is distinct. First, the RKKY interactions are more complex because of the novel electronic structure in quasiperiodic systems [24–29]. Second, one may envision a non-random placement of the local moments: quasicrystals are characterized by a set of local environments arranged in a non-periodic fashion, which can be labeled by the number of nearest neighbors z . It is then reasonable to assume that it would be energetically more favorable for the local moments to sit at a particular local environment, which could favor ordered magnetic states over the glassy state [30–32].

The majority of experiments identify spin-glass order in quasicrystals [33–37]. However, important differ-

ences are present in the periodic approximations to the quasicrystals, known as approximants, where long-range magnetic order is often reported [34, 36, 37], indicating a non-trivial role of the system unit-cell size.

We follow Refs. [30, 31] to study the ordering of local moments placed in a magnetic quasicrystal and model the local moments as Ising spins for convenience. We work mainly on the square approximants of the two-dimensional octagonal or Ammann-Beenker tiling [38–40], but show that our results also hold for the Penrose motif. We assume the spins occupy a particular local environment of the quasicrystal, determined by the number of nearest neighbors z , and interact via an average RKKY interaction [41], which we compute using the Kernel Polynomial Method (KPM) [42]. Using large-scale Monte Carlo (MC) simulations, we find long-ranged magnetic order for most of the parameters considered. However, the order is fragile: a fraction of the sites experience a zero exchange field and keep fluctuating down to $T \rightarrow 0$, implying an extensive ground state entropy and enhanced sensitivity of this magnetic state towards perturbations.

In the complementary limit of diluted spins, we investigate spin-flip relaxation rate between the local magnetic moments and the conduction electrons at the Fermi level. This quantity, measured via electron spin resonance (ESR) [43], gives direct access to the local quasicrystalline electronic environment. We compute its evolution with the approximant size and show that it may increase or decrease, depending on the position of the electrons’ Fermi level. Applying our results to recent experimental data [36], we conclude the Fermi energy of the conduction electrons is most likely located close to a pseudogap in the density of states of the quasicrystal, because the relaxation rate diminishes as we go from the approximant to the quasicrystal.

The paper is organized as follows. In Sec. II, we discuss the electronic properties of the Ammann-Beenker tiling and the resulting RKKY interactions calculated via the KPM. In Sec. III, we discuss the magnetic model for Ising spins placed on a given local environment of this tiling. We perform large-scale Monte simulations to character-

ize the resulting magnetically ordered states and discuss their peculiarities. In Sec. IV we briefly discuss that our scenario also holds in the Penrose lattice. In Sec. V, we discuss the spin-flip relaxation rate when the local moments are coupled to the quasicrystalline electronic bath in the limit of diluted impurities. Finally, we connect our results to experimental results and conclude the paper in Sec. VI. In Appendix A, we discuss the robustness of our minimal magnetic model with respect to extra exchange terms.

II. ELECTRONIC STATES AND MAGNETIC COUPLINGS

A. Tiling

As a minimal model for a quasicrystal, we consider the Ammann-Beenker tiling shown in Fig. 1(a). This tiling contains 45° rhombuses and squares as building blocks and six distinct local environments with coordination numbers $z = 3, \dots, 8$. In Fig. 1(a), we highlight the sites with $z = 3$. These environments correspond to the following fraction of the total number of sites N in the system f_z : $f_3 = 1/s$, $f_4 = 2/s^2$, $f_5 = 2/s^3$, $f_6 = 2/s^4$, $f_7 = 1/s^5$, and $f_8 = 1/s^4$, where $s = 1 + \sqrt{2}$ is the silver ratio. We follow Ref. [40] and generate square approximants to this tiling with $N = 239, 1393, 8119, 47321, 275807, 1607521$ sites, and linear size $L_k = s^k$, with the integer k ranging from 3 in the approximant $N = 239$ to 8 in the mosaic $N = 1607521$.

Experimentally, an approximant is the periodic repetition of a unit cell containing a finite portion of the quasicrystal. The unit cell size can be taken as the effective size of the approximant since all quasiperiodicity comes from it. For an infinite-sized unit cell, one recovers the true quasicrystal. In this work, we will consider finite tilings with open boundary conditions as our approximants to the true quasicrystal. In principle, different constructions are possible, for instance, taking small subsets of the quasicrystal and repeating them periodically, a situation closer to the experimental one. Periodic boundary conditions usually lead to a faster approach to the thermodynamic limit because they avoid a variable coordination number at the sample boundaries, for instance. In quasicrystals, we have an intrinsic distribution of z and employing periodic boundary conditions does not necessarily lead to a faster convergence to the thermodynamic limit. Moreover, as we will show in Sec. III, we recover the usual finite size scaling of thermodynamic quantities using our definition of approximants with open boundary conditions [44, 45].

We focus on the most frequent local environments of the Ammann-Beenker tiling, those with $z = 3$ and $z = 4$. Moreover, they can be related to other z in different approximants by the inflation/deflation symmetry: selecting a subset of vertices of the approximant (say all sites

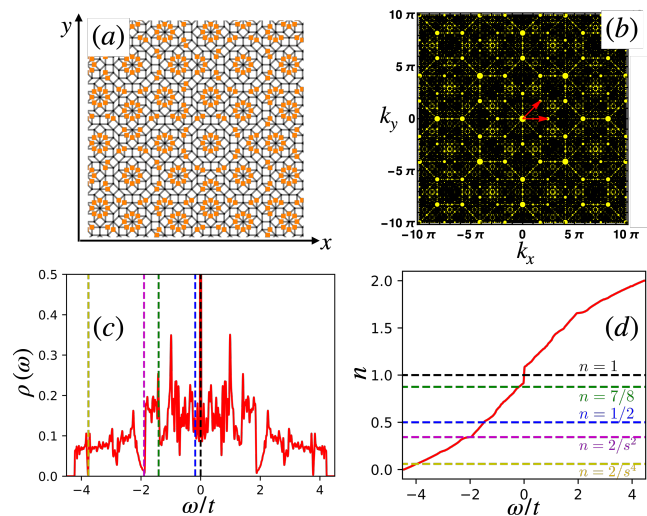


Figure 1. Structural and electronic properties of the two-dimensional tiling. (a) The Ammann-Beenker tiling. The squares highlight sites with coordination number $z = 3$; (b) Structure factor for the $N = 8119$ approximant considering only the sites with $z = 3$. The width of the dots is proportional to their intensity. The arrows correspond to the reciprocal vectors $\pi(1, 0)$ and $\pi(1/\sqrt{2}, 1/\sqrt{2})$, which originate at the Γ point; (c) Density of states, $\rho(\omega)$, as a function of the energy, ω/t , for the $N = 1607521$ approximant considering nearest-neighbor hopping t only; (d) Electronic filling as a function of ω/t . The horizontal dashed lines highlight the fillings n considered in this work. $s = 1 + \sqrt{2}$ is the silver ratio;

with a given z) and joining them by new edges yields a similar (rescaled) quasiperiodic tiling [38, 41]. Consider, for instance, sites with $z = 4$. If we join them and scale the resulting tiling by s , we recover the $z = 6$ sites of the next approximant. In the same fashion, the $z = 3$ sites map into (part of) the $z = 5$ sites. If we inflate an approximant twice, we recover all $z = 8$ sites of the second next approximant.

In Fig. 1(b), we show the Fourier transform of the sites with $z = 3$ in the $N = 8119$ approximant: $|\sum_j e^{-i\mathbf{r}_j \cdot \mathbf{k}}|^2 / N$, where \mathbf{k} are the momentum and \mathbf{r}_j the position of the site j in the tiling. The brightest Bragg peaks closest to the Γ point are located at a distance π in units where the lattice spacing $a = 1$. If we consider all N sites in the approximant, these peaks are instead located at a distance $s\pi$. Therefore, focusing on the $z = 3$ sites only, we effectively rescale the lattice spacing by a factor s , indicating that the effective neighbor distance of the quasicrystal is increasing. The inflation/deflation property thus guarantees the 8-fold rotational symmetry of the approximant, even when considering only a specific subset of sites.

B. Electronic states

We model the electronic properties of this tiling considering a nearest-neighbor tight-binding Hamiltonian

$$H_0 = -t \sum_{\langle ij \rangle, \sigma} \left(c_{i\sigma}^\dagger c_{j\sigma} + c_{j\sigma}^\dagger c_{i\sigma} \right), \quad (1)$$

where $c_{j\sigma}^\dagger$ ($c_{j\sigma}$) creates (destroys) an electron of spin σ at site j . t is hopping amplitude between nearest neighbors and is restricted to the sides of the rhombuses and squares [39]. We measure all energies in terms of t , and the half-bandwidth is $\approx 4t$, comparable to the one in the square lattice, which is reasonable given that the average value of z is 4. As we use open boundary conditions, we preserve the particle-hole symmetry of this (bipartite) tiling and the spectrum is symmetric with respect to $\omega = 0$, allowing us to work solely with fillings $n \leq 1$. In principle, by quadrupling the tiling size, it is possible to employ periodic boundary conditions while preserving the bipartiteness of the approximants [46]. In this work, we refrain from using this numerically more expensive approach.

We employ the KPM [42] to compute the spectral properties of large approximants. This method was successfully applied in the previous studies of disordered [47–49] and quasicrystalline [50] systems, and is capable of resolving the low-energy features of these systems. Within the KPM, the (rescaled) local density of states is given by

$$\rho_{ii}(\tilde{\omega}) = \frac{1}{\pi\sqrt{1-\tilde{\omega}^2}} \left[g_0 \mu_0^{ii} + 2 \sum_{m=1}^M g_m \mu_m^{ii} T_m(\tilde{\omega}) \right], \quad (2)$$

where $T_m(\tilde{\omega})$ is the m -th Chebyshev polynomial, M is the number of moments in the expansion, and g_m is the Jackson Kernel [42], introduced to dampen the Gibbs oscillations due to a finite M . The expansion moments are defined as $\mu_m^{ij} = \langle i | T_m(\tilde{H}) | j \rangle$, where \tilde{H} is the renormalized Hamiltonian with its spectrum $\in [-1, 1]$. The density of states can, in principle, be computed as $\rho(\tilde{\omega}) = \sum_i \rho_{ii}(\tilde{\omega}) / N$, which amounts to compute $\sum_i \langle i | T_m(\tilde{H}) | i \rangle = \text{Tr}[\mu_m^{ij}]$. For large system sizes, the exact evaluation of traces is time-consuming, and we resort to its stochastic estimation: $\text{Tr}[\mu_m^{ij}] = \sum_{r=1}^R \langle r | T_m(\tilde{H}) | r \rangle / R$, where $|r\rangle$ is a random vector and R is their number. The advantage of this method is that we can use $R \ll N$ with its error decreasing as $1/\sqrt{NR}$ [42].

In Fig. 1(c) we show $\rho(\omega)$ for $N = 1607521$ sites and $R = 10$. We can observe the key features of the Ammann-Beenker tiling: (i) pseudogaps at energies corresponding to the fillings $n = 2/s^4$ and $n = 2/s^2$, Fig. 1(d); (ii) the divergence of $\rho(\omega = 0)$, due to localized states; and (iii) the spiky nature of the $\rho(\omega)$ as a function of ω [2, 39, 51]. The fact that these key features are captured

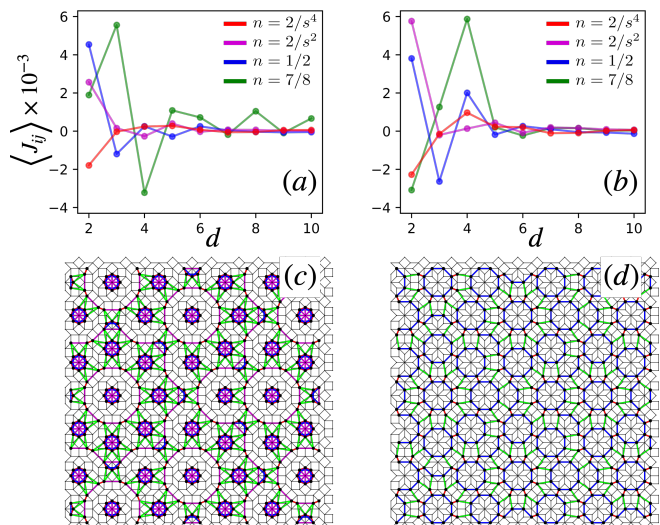


Figure 2. Average value of the RKKY coupling in Eq. (4), for several fillings n and for sites with (a) $z = 3$ and (b) $z = 4$. We considered $N = 8119$, $J_0 = t = 1$, and d is the Manhattan distance $d = |\Delta x| + |\Delta y|$, where Δx (Δy) is the difference in the x (y) coordinates of the sites i and j . Minimal set of exchange couplings for the $N = 1393$ tiling. (c) $z = 3$. Four magnetic exchange couplings: J_1 (red), J_2 (blue), J_3 (green) and J_4 (magenta). (d) $z = 4$. Three couplings: J_1 (red), J_2 (blue), and J_3 (green).

indicates that the KPM is well suited to describe the non-trivial spectral dependence of the electronic states in quasicrystal approximants, up to their finite size resolution.

C. Magnetic model

Our main motivation is to describe the fate of local magnetic moments in contact with a quasicrystalline electronic bath. Because quasicrystals display a distribution of local environments, we consider that the magnetic moments are not randomly placed but instead occupy all sites with a given z . We model these moments as a spin- S and couple them to the local spin density of the conduction electrons via an exchange coupling J_0 . To generate a spin-only model, we integrate out the conduction electron and write

$$H = \frac{1}{2} \sum_{i \neq j} J_{ij} S_i S_j, \quad (3)$$

where $S_i = \pm 1$ and the interaction between spins J_{ij} is [47]

$$J_{ij} = -2J_0^2 \int_{E_F}^D d\omega \int_{-D}^{E_F} d\omega' \frac{\rho_{ij}(\omega) \rho_{ji}(\omega')}{\omega - \omega'}, \quad (4)$$

where D is the electronic half-bandwidth, E_F is the Fermi energy, and $\rho_{ij}(\omega)$ is given in Eq. (2). We consider

$T = 0$ and $M \sim 10^3$ KPM moments to evaluate J_{ij} . A few comments are in place: (i) Instead of considering the Heisenberg model, we study the simpler Ising model. This is motivated by the studies of spin glasses [23], where the key aspects of the local moment freezing are already captured by Eq. 3; (ii) We include the effects of the conduction electrons at second order in J_0 as we expect Eq. 3 to qualitatively describe the ordering of local moments in a quasicrystalline metallic environment. This is physically motivated by the observation that, although the impurities alter the electronic states of the bath, as long as the conduction electrons remain metallic, the key features of the effective magnetic couplings are captured perturbatively.

We show the average value of the coupling J_{ij} for a given local environment in Figs. 2(a) and 2(b). As discussed previously in Refs. [30, 31], J_{ij} has a complex spatial and filling dependence. To obtain the full set of J_{ij} required for the MC simulations of Eq. (3) is a challenging task, and we are restricted to $N \leq 8119$ approximants, even within KPM. This hampers a conclusive finite-size scaling study of putative ordered states. Moreover, J_{ij} might display appreciable values for distant sites [52], further complicating a finite-size study.

To overcome these challenges, we employ a simpler model, following Ref. [41]. Given a subset of sites, say sites with $z = 3$ or $z = 4$, we consider a minimal set of exchange couplings generating unbounded clusters at $T = 0$ and therefore allowing for long-range order, Figs. 2(c) and 2(d). For the $z = 3$ environment, we implement this set with an exchange coupling J_1 across the short diagonal of the rhombus, a coupling J_2 across two neighboring rhombi, an exchange J_3 across neighboring square and rhombus, and a coupling J_4 across two squares, or rhombi, edges. The pattern formed by this choice of couplings is displayed in Fig. 2(c), where we see it percolates the lattice but still leaves a fraction of the sites surrounding the $z = 8$ sites weakly coupled to the bulk.

For $z = 4$, the set of couplings is displayed in Fig. 2(d). Here, we consider the J_1 coupling across the short diagonal of the rhombus, a coupling J_2 across the square diagonal, and the J_3 coupling across neighboring squares and rhombi. There are no large clusters of disconnected structures for this minimal choice of couplings. From now on, we set J_1 as our energy scale.

We consider the value of these exchange couplings as the average value of the corresponding RKKY interaction for the $N = 47321$ approximant. This approximant size is now amenable to KPM calculations because we focus on a restricted subset of couplings. In Fig. 3, we show the histogram of the minimal set of exchange couplings for $z = 3$ and $n = 2/s^2$. $P(J)$ is bounded and has a similar width for all neighbors, with its mean value capturing the correct energy scale of the problem. Therefore, the minimal model retains the chief ingredients to describe the order of local moments embedded in a metallic quasicrystal. In Appendix A, we show that the inclusion of extra couplings does not alter the conclusions presented

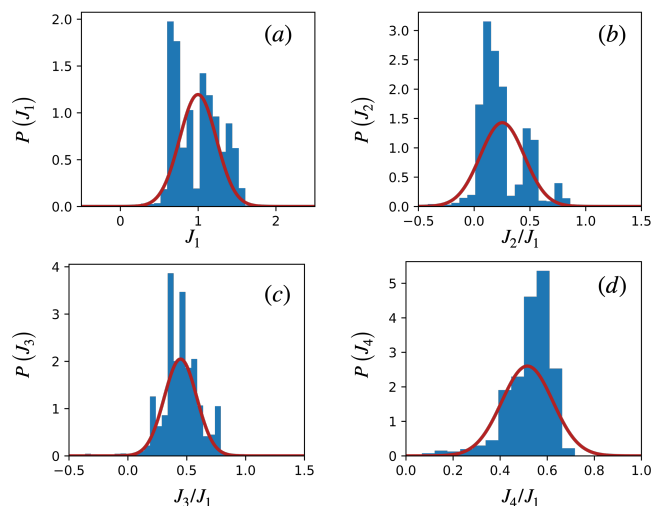


Figure 3. Histogram of exchange couplings values for $z = 3$ and $n = 2/s^2$. We normalize the couplings with respect to J_1 . We superimpose a Gaussian fit with the average values of Tab. I and variances: (a) $P(J_1)$, $\sigma_1 = 0.33$; (b) $P(J_2)$, $\sigma_2 = 0.28$; (c) $P(J_3)$, $\sigma_3 = 0.20$; and (d) $P(J_4)$, $\sigma_4 = 0.15$.

n	J_1	J_2	J_3	J_4
$2/s^4$	-1	-0.501	-0.163	-0.321
$2/s^2$	1	0.255	0.449	0.518
$1/2$	1	-0.389	-0.435	0.042
$7/8$	1	0.666	0.682	0.559

Table I. Exchange couplings J_i for $z = 3$ and different fillings n . $|J_1|$ sets the scale.

in the main text.

III. MAGNETIC ORDER

We now discuss the magnetic states of Ising spins interacting with the averaged RKKY couplings in Tabs. I and II, corresponding to four different fillings n of the conduction electrons. To solve Eq. (3), we employ classical MC simulations on approximants with $N = 239, 1393, 8119, 47321$ and open boundary conditions. Within our scheme, system size and aperiodicity are intertwined. As we increase N , we increase the effective size of the approximant unit cell, and the limit $N \rightarrow \infty$ corresponds to the quasicrystal. We perform equilibrium MC simulations combining single-site Metropolis updates with the parallel tempering method [53, 54]. Usually, we perform 10^5 Monte Carlo steps for thermalization and 5×10^5 Monte Carlo steps for measurements.

To characterize long-ranged ordered phases, we compute the staggered magnetization for a single Monte Carlo snapshot $\mathcal{M}_s = \sum_i \zeta_i S_i / N$, with the Monte Carlo order parameter given by $m_s = \sqrt{\langle \mathcal{M}_s^2 \rangle}$, where $\langle \dots \rangle$ de-

n	J_1	J_2	J_3
$2/s^4$	-1	-0.971	-0.342
$2/s^2$	1	0.379	-0.056
$1/2$	-1	3.242	-3.701
$7/8$	-1	-0.831	0.813

Table II. Same as Tab. I but now for $z = 4$.

notes the Monte Carlo average. The local phase $\zeta_i = \pm 1$ describes the ordered ground state spin configuration, and we will explain how we determine it shortly. To capture the ordering temperature T_N , we employ the Binder cumulant $B_s = 3/2 - \langle \mathcal{M}_s^4 \rangle / 2 \langle \mathcal{M}_s^2 \rangle^2$, normalized such that $B_s \rightarrow 1$ in the ordered phase and $B_s \rightarrow 0$ in the disordered phase. The crossing point of the curves $B_s \times T$ for different systems sizes determines T_N [54]. To track possible spin freezing without long-range order, we also compute the Edwards-Anderson order parameter [23, 55]: $q_i = (1/\tau) \int_0^\tau S_i(0) S_i(\tau)$, with τ the Monte Carlo simulation time, measured after the equilibration. From this definition, we see that q_i is the overlap of a spin with itself at a later time. In a paramagnetic phase, $q \rightarrow 0$ because the spins fluctuate over time. If the spins are frozen in an ordered state, we have both $q \neq 0$ and $m_s \neq 0$. For a spin-glass state, $q \neq 0$ and $m_s = 0$.

To calculate the local phases ζ_i , corresponding to the spin configuration in the ground state, we proceed as follows: (i) we perform Monte Carlo runs at low temperatures and generate 10^3 independent spin configurations; (ii) we express Eq. (3) as $H = \sum_i S_i h_i / 2$, with the local (exchange) field defined as $h_i = \sum_j J_{ij} S_j$. We sequentially sweep the lattice and iteratively anti-align a given spin with h_i until the change in the spin configuration after the sweep is smaller than a given tolerance value; (iii) out of the original 10^3 states, we select the spin configuration with the lowest energy as the global ground state. This particular state defines the local phases ζ_i in our simulations for a given set of parameters [30, 31].

The Ammann-Beenker tiling is bipartite, as illustrated by the particle hole symmetric density of states in Fig. 1(c). If we place Ising spins on all approximant sites and allow them to interacting with each other via a nearest-neighbor antiferromagnetic coupling J_1 , we get a Néel ground state [45, 56, 57] below $T_N/J_1 = 2.386(2)$. Therefore, a dense quasiperiodic lattice of local moments can sustain regular long-range order [36].

A. $z = 3$ sites

We start discussing the situation where the magnetic impurities are placed in all sites with $z = 3$, corresponding to a fraction of $f_3 = 1/s = 0.414$ of the N sites in an approximant, see Fig. 1(a). The corresponding magnetic coupling structure is in Fig. 2(c), with the corresponding J_i values in Tab. I.

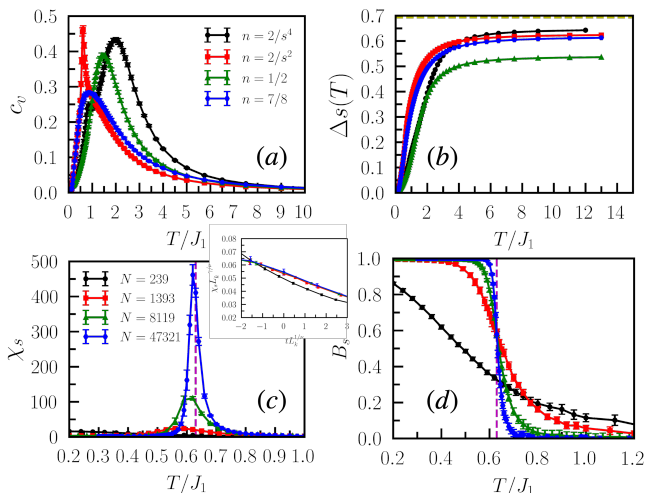


Figure 4. Monte Carlo results for local moments placed at sites with $z = 3$ local environments in the Ammann-Beenker tiling. (a) Specific heat c_v as a function of temperature T for four different conduction electron fillings n and $N = 8119$. (b) Residual entropy $\Delta s(T)$, per site, as a function of T for $N = 8119$. The dashed line gives $s(T \rightarrow \infty) = \log 2$. The curve labels are the same as in (a). (c) Susceptibility associated with the staggered magnetization χ_s as a function of T for $n = 2/s^2$ and different N . The vertical dashed line marks the position of the ordering temperature T_N . Inset: Finite scaling of the data. Here, $t = (T - T_N)/T_N$ is the reduced temperature, L_k is the linear size of the approximant (see text), and we consider the critical exponents corresponding to the two-dimensional Ising universality class: $\gamma = 7/4$ and $\nu = 1$. (d) Binder cumulant B_s of the order parameter as a function of T for $n = 2/s^2$. The dashed line marks the crossing of the curves for $N \geq 1393$ and determines $T_N = 0.63(1) J_1$. The curve colors are the same as in (c).

The specific heat displays a peak for all electronic fillings n considered in this study, Fig. 4(a). The peak position depends on n since the magnetic couplings are a function of n . We estimate the residual entropy, per spin, as $\Delta s(T) = \int_0^T (c_v/T) dT = s(T) - s_0$. For an ordinary ordered system, we expect $s_0 \rightarrow 0$ and $s(T \rightarrow \infty) \rightarrow \log 2$. Fig. 4(b) shows that Δs never saturates to $\log 2$, indicating a residual ground state entropy, per site, $s_0 \neq 0$. If we ascribe this residual entropy to the weakly coupled clusters of spins with $z = 3$ surrounding the $z = 8$ sites [30, 31], we can estimate the ground state degeneracy, per spin, as $g_0 \approx (1/4) \times 8f_8/f_3 = 2/s^3$. The factor of $1/4$ comes from the fact that about $1/4$ of these clusters are weakly coupled, Fig. 2(c). This amounts to $\Delta s(T \rightarrow \infty) = \log 2 (1 - 2/s^3) \approx 0.59$, which corresponds roughly to the values presented in Fig. 4(b) for all fillings but $n = 1/2$. This last case is special because here $J_4 \approx 0$, enhancing the ground-state degeneracy.

To corroborate this picture, we study the spatial structure of the spin overlap q_i for a given temperature T , Fig. 5. We observe that for $T > T_N$, $q_i \approx 0$ for all sites. As the temperature decreases, q_i increases, suggesting an or-

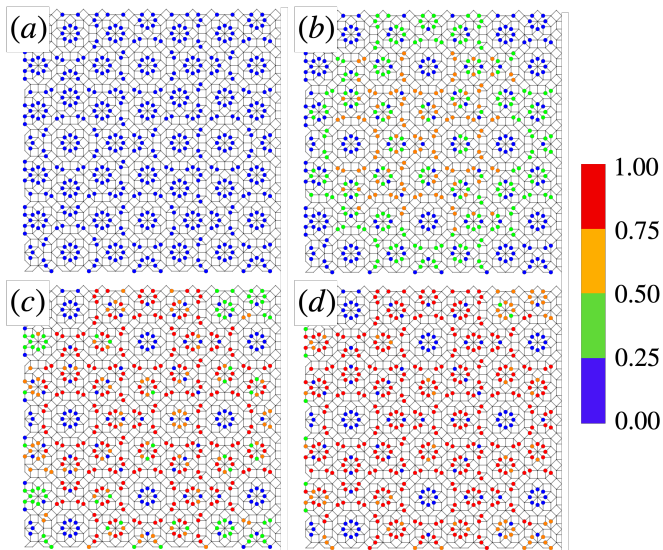


Figure 5. Spatial distribution of the Edwards-Anderson order parameter q_i , at different temperatures, for local moments placed at sites with $z = 3$ local environments in the Ammann-Beenker tiling. (a) $T = 0.60J_1$; (b) $T = 0.50J_1$; (c) $T = 0.30J_1$, (d) $T = 0.20J_1$. Here we considered $n = 2/s^2$, $N = 1393$, and $T_N = 0.63(1)J_1$ for this parameter set. The color defines the value of q_i .

dered state. However, even at low- T , roughly a quarter of the $z = 3$ sites surrounding the $z = 8$ sites show $q_i \approx 0$, indicating that they indeed fluctuate despite the bulk of the spins being ordered.

Fig. 4(c) shows the susceptibility associated with the staggered order parameter for the electronic filling $n = 2/s^2$. Even though $s_0 \neq 0$, the system orders, as indicated by the enhancement of the peak in χ_s as we increase the system size. The Binder cumulant captures this critical behavior in Fig. 4(d), with the curves for different N crossing at the ordering temperature $T_N = 0.63(1)J_1$. The curve for $N = 239$ contains too few spins and suffers from strong finite-size corrections, crossing the other curves at different points. The Curie-Weiss temperature for this parameter set is $\theta_{CW} \approx -3J_1$, implying the frustration pushes the ordered temperature down by a factor of 5 compared to this scale. With the value of T_N , we check that χ_s follows the usual finite-size scaling with the critical exponents for the two-dimensional Ising universality class, inset of Fig. 4(c) [44, 45, 56, 58, 59]. We then conclude that the magnetic transition survives for $N \rightarrow \infty$, ruling out, for instance, the existence of an intrinsic spin-glass phase.

Most magnetic moments develop a long-range order while a small fraction of the spins keep fluctuating at low temperatures. This is similar to partially ordered states identified in frustrated magnets. It happens because the ordered spins do not exert any mean field on the remaining disordered ones, and thermal fluctuations are unable to lift this degeneracy [60–65].

We investigate the resulting ordered states via the

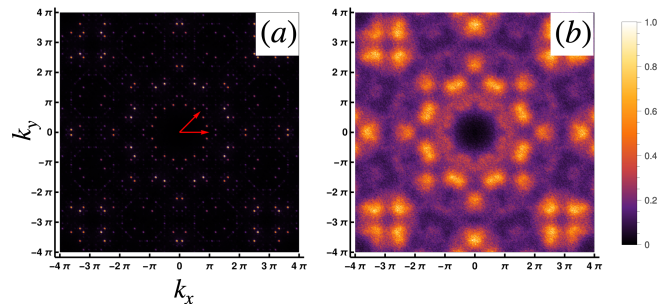


Figure 6. Static spin structure factor for local moments placed at sites with local environments $z = 3$. We consider $N = 8119$ and $n = 2/s^2$. (a) $T = 0.5J_1 < T_N$. (b) $T = 1.0J_1 > T_N$. The red arrows are the same as in Fig. 1(b). The color code in each figure is independently normalized.

static spin structure factor, $\langle \left| \sum_j S_j e^{-ir_j \cdot k} \right|^2 \rangle / N$, with representative results in Fig. 6. Above the ordering temperature, the structure factor displays the 8-fold symmetry inherited from the tiling with the Bragg-like peaks broadened by the temperature. For $T < T_N$ the brightest peaks split into two, and their position does not coincide with the structural peaks in Fig. 1(b), indicating the emergence of a complex antiferromagnetic arrangement of the local moments. The existence of well-defined bright peaks at low- T also confirms that the fluctuating spins occupy well-defined positions in the lattice. A typical ground state with local moments displaying long-range antiferromagnetic order is shown in Fig. 7(a). This state defines the local phases $\zeta_i = \pm 1$.

An useful way of studying the behavior of local quantities in a quasicrystal is to consider the so-called perpendicular space [19, 66]. Within the cut and project method, Ref. [40], we consider a parent 4-dimensional cubic lattice which has two orthogonal bidimensional planes, called the physical and the perpendicular planes, both symmetric under 8-fold rotations. The approximant tilings are in the physical space. The perpendicular space organizes the sites according to their local environment. Because in our work we consider a subset of z , we select the corresponding regions in this space. A plot of the ground state magnetization for two system sizes, with $z = 3$ sites and $n = 2/s^2$ is shown in Fig. 8. No immediate pattern, or significant size dependence, is visible inside each region indicating that the local value of the magnetization depends on a complex balance between the tiling geometry and the frustration induced by the magnetic couplings. Therefore, we focus on analyzing the results in real or physical space.

We start by investigating the distribution of the Edwards-Anderson order parameter, $P(q)$, Fig. 7(b). This histogram is constructed considering the values of $q = \sum_i q_i / N$ for different configurations, as those of Fig. 5, at several Monte Carlo times τ . For $T > T_N$, the spins are fluctuating and $P(q)$ is peaked at $q = 0$, see also Fig.

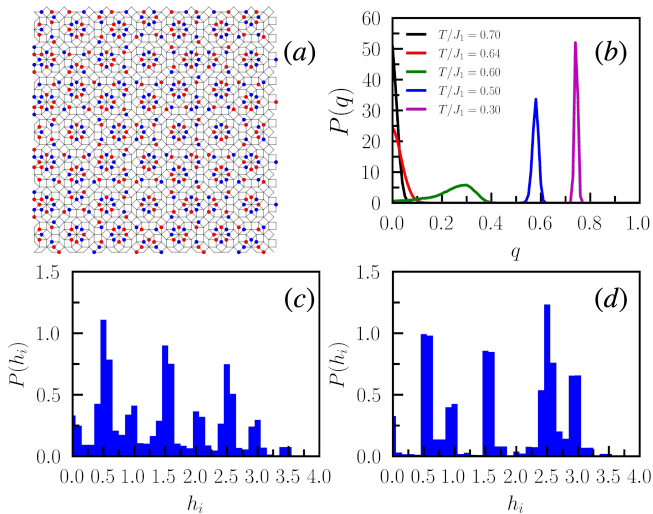


Figure 7. Characterization of the ordered states for local moments placed at the $z = 3$ sites and $n = 2/s^2$. (a) Ground state configuration for $N = 1393$. The different colors indicate opposite spin orientations defining the local phases $\zeta_i = \pm 1$ (see text). (b) Histogram of the Edwards-Anderson order parameter $P(q)$ for different temperatures T . Histogram of the local exchange field, $P(h_i)$: (c) $T = J_1 > T_N$ and (d) $T = 0.3J_1 < T_N$. $P(q)$ and $P(h_i)$ are both symmetric with respect to zero due to time reversal symmetry. Therefore, we consider only positive values of q and h_i .

5(a). For $T < T_N$, $P(q)$ peaks at $q \neq 0$, indicating the gradual freezing of the spins into the ordered state; see also Figs. 5(b)-(d). Because a fraction of the spins continue fluctuating to very low temperatures, $P(q)$ peaks at values $q < 1$ even at the lowest T , thus accounting for a non-vanishing residual entropy s_0 . In our simplified model, we always detect a single peak in $P(q)$, signaling a unique ground state up to symmetry-allowed operations [30, 31].

Alternatively, we investigate the ordered state via the distribution of local, or mean, fields $h_i = \sum_j J_{ij} S_j$, which corresponds to the density of states of Eq. (3). The histograms $P(h_i)$ in Figs. 7(c) and (d) display many peaks, indicating an intricate local field distribution due to the combination of quasiperiodicity and a complex ordered state, Fig. 7(a). Importantly, even for $T < T_N$, we observe $P(h_i \rightarrow 0) \neq 0$, corroborating the presence of fluctuating spins inside the ordered phase.

Taken together, these facts point toward a fragile, long-range, ordered state. Because $P(h_i \rightarrow 0) \neq 0$, perturbations will couple directly to the loose spins, and those at small but finite h_i , profoundly affecting the ordered state even at weak coupling [37]. To illustrate this point, we dilute a fraction x of the spins in a given sample. We also average our results over different vacancy configurations in these simulations, typically 100. In Fig. 9(a), we observe that the specific heat peak is rounded and becomes broader as we increase the vacancy concentration, a typical signature of a glassy state [23].

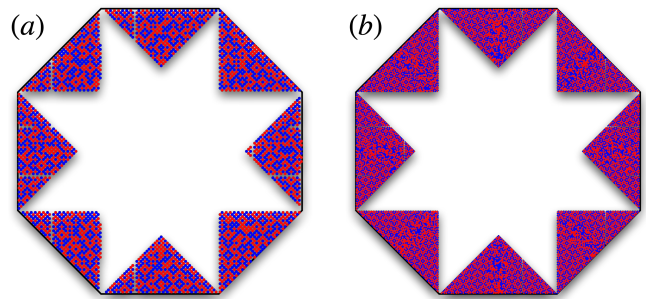


Figure 8. Characterization of the ordered states for local moments placed at the $z = 3$ sites and $n = 2/s^2$ in the perpendicular space for (a) $N = 8119$ and (b) $N = 47321$. The different colors indicate opposite spin orientations. We exclude the sites sitting at the open boundaries.

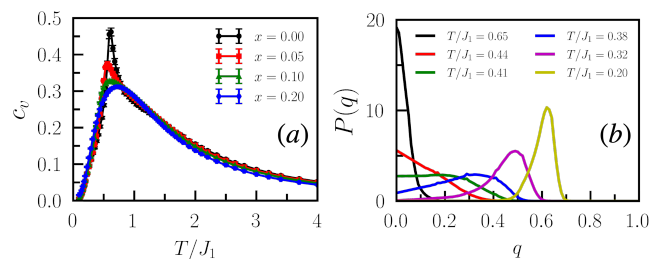


Figure 9. Monte Carlo results for local moments placed at $z = 3$ local environments, $N = 8119$, and $n = 2/s^2$. (a) c_v as a function of T for different values of dilution x . (b) $P(q)$ for $x = 0.10$ and different T values.

A peak in the specific heat marks the location of a relevant microscopic energy scale in the problem. In a spin glass, we have a distribution of energy scales due to the quenched disorder, and thus, we expect a broad peak in the specific heat. Moreover, as we no longer have a transition from a paramagnetic state to an ordered state, with the accompanying substantial release of entropy, the peak in the specific heat becomes rounded. We confirm the presence of a glass-like nature of the magnetic state by investigating $P(q)$. At not-too-low temperatures, it peaks at $q \neq 0$ and a tail extending to a finite value at $q = 0$ [67]. As we further reduce the temperature, the correlation length becomes comparable to the system size, causing $P(q)$ to display a broad peak at $q < 1$ [68].

B. $z = 4$ sites

We present sample results for placing local moments at sites with $z = 4$ neighbors. They correspond to a fraction $f_4 = 2/s^2 = 0.343$ of all sites in a given approximant. Sites with $z = 3$ are particular because they display weakly connected islands around the $z = 8$ sites. Sites with $z = 4$ form a more connected network of interacting spins, Fig. 2(d). The corresponding values of the magnetic couplings are presented in Tab. II.

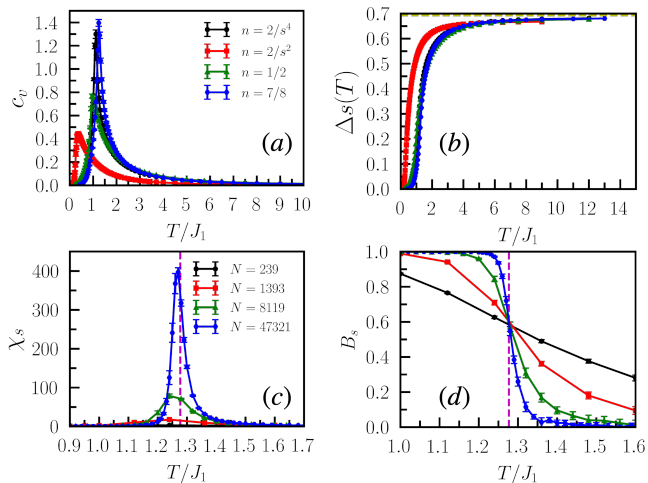


Figure 10. Monte Carlo results for local moments placed at $z = 4$ local environments. (a) Specific heat c_v as a function of T for four n and $N = 8119$. (b) Residual entropy $\Delta s(T)$, per site, as a function of T for $N = 8119$. The dashed line gives $s(T \rightarrow \infty) = \log 2$. The curve labels are the same as in (a). (c) χ_s as a function of T for $n = 7/8$. The vertical dashed line marks the ordering temperature's position T_N . (d) Binder cumulant B_s as a function of T for $n = 7/8$. The dashed line marks the crossing of the curves and determines $T_N = 1.277(5)J_1$. The curve colors are the same as in (c).

Fig. 10(a) shows the specific heat as a function of the temperature. Compared to Fig. 4(a), the peaks are more pronounced, indicating more robust ordered states. This is confirmed in Fig. 10(b), where we see that the residual entropy s_0 is tiny. Using MC simulations, it is hard to pinpoint the precise value of s_0 when it is small [69], and we take $s_0 \approx 0$.

A representative study of the ordering is shown in Figs. 10(c) and (d) for $n = 7/8$. The staggered susceptibility displays a well-defined peak close to the ordering temperature $T_N/J_1 = 1.277(5)$, which we extract via the crossing of the Binder cumulant. Here, even the curve from the smallest system size crosses all the others at T_N , indicating milder finite size effects than the $z = 3$ case. The Curie-Weiss temperature for this parameter set is $\theta_{CW} \approx 2.5J_1$, implying the effects of frustration are not so severe despite the lack of periodicity and competing magnetic interactions.

The ground state for $n = 7/8$ is shown in Fig. 11(a). It displays islands of spins up (down) surrounded by islands of spin down (up), with the spins across the rhombus short diagonal parallel to each other. The structure factor at finite temperature is shown in Fig. 11(b), with the sharpest Bragg-like peaks displaying the 8-fold symmetry and no splitting, reflecting the ordered state's local ferromagnetic structure. To gauge the robustness of the ordered state for $n = 7/8$, we compute $P(h_i)$, Fig. 11(c) and (d). We observe that the number of peaks and the relative contribution of the peak at $h_i \rightarrow 0$ are smaller than those in Fig. 7. This is consistent with a more ro-

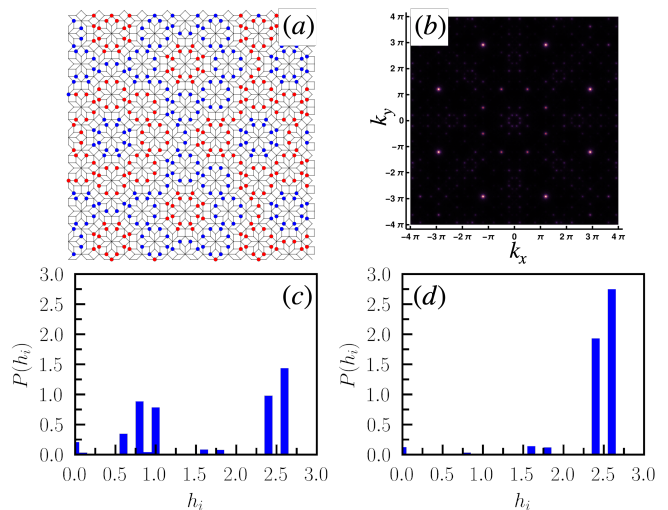


Figure 11. Characterization of the ordered states for local moments placed at the $z = 4$ sites and $n = 7/8$. (a) Ground state configuration for $N = 1393$. The different colors indicate opposite spin orientations. (b) Static spin structure factor for $N = 8119$ and $T/J_1 = 1.2$. The color scale is the same used in Fig. 6. Histogram of the local exchange field, $P(h_i)$: (c) $T = 1.4J_1$ and (d) $T = 0.5J_1$.

bust and simpler ordered pattern, signaled by the absence of weakly coupled spin-cluster and $s_0 \approx 0$. Because the system is frustrated, the disorder will eventually melt the ordered state [70–72], but one expects a less pronounced effect in comparison to the $z = 3$ case.

IV. PENROSE LATTICE

To gauge the generality of our results, we study Eq. (3) in the Penrose tiling. Again, open boundary conditions are considered. We show sample results in Fig. 12 where we consider $n = 7/8$ and the spins placed at sites with $z = 3$ neighbors. The minimal set of exchange couplings is displayed in Fig. 12(a), with the ground state illustrated in Fig. 12(b). We also obtain an intricate ordered ground state, and although the specific heat in Fig. 12(c) does not show a well-defined peak, the residual entropy is tiny. We can confirm it first by studying $P(q)$ in Fig. 12(d). For $T > T_N$, $P(q)$ is peaked around $q = 0$. As the temperature decreases, the peak of $P(q)$ moves towards $q \approx 1$.

We show snapshots of the system configurations in Fig. 13 at temperatures below T_N . Spins surrounding sites with $z = 5$ fluctuate inside the ordered phase, but their number is strongly suppressed as $T \rightarrow 0$, consistent with $s_0 \approx 0$. Although their contribution to the thermodynamic response of the current system is minor, it is worthwhile to note that the existence of partial order is a robust and general phenomenon for local moments diluted in metallic quasicrystals. On the other hand, it points to the general conclusion that the combination

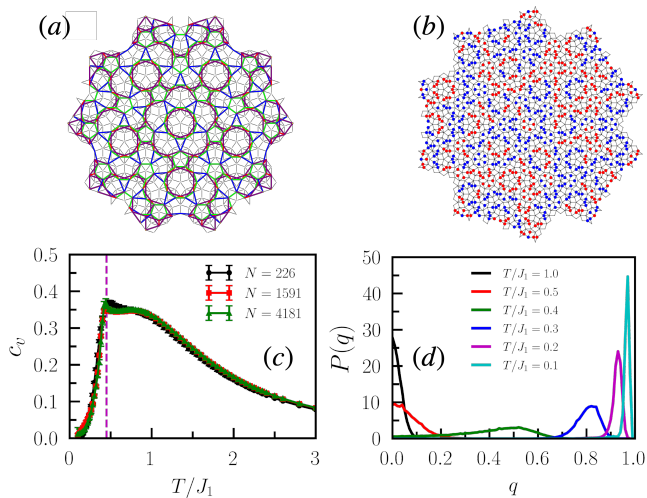


Figure 12. Monte Carlo results for local moments placed at $z = 3$ local environments in the Penrose lattice. (a) Minimal set of exchange couplings for the $N = 1591$ tiling with four magnetic exchange couplings: J_1 (red), J_2 (blue), J_3 (green) and J_4 (magenta). (b) Ground state configuration for $N = 1591$, $n = 7/8$, and $J_2 = -0.308J_1$, $J_3 = 0.442J_1$, $J_4 = 0.028J_1$. The different colors indicate opposite spin orientations. (c) Specific heat as a function of temperature for different approximant sizes. The vertical dashed line marks the ordering temperature's position $T_N = 0.45(1)J_1$. (d) Histogram of the Edwards-Anderson order parameter $P(q)$ for different temperatures T .

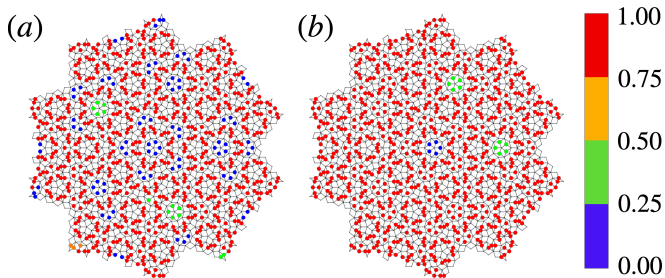


Figure 13. Snapshots of the spatial distribution of the Edwards-Anderson order parameter q_i for local moments placed at sites with $z = 3$ local environments in the Penrose tiling: (a) $T = 0.1J_1 < T_N$ and (b) $T = 0.01J_1 < T_N$. We consider the same parameters as in Fig. 12.

of deterministic quasiperiodicity and frustration is not enough to generate a spin-glass state within our minimal model and that true randomness is required.

V. LOCAL MOMENT RELAXATION RATE

Ref. [36] presents a detailed ESR study in of rare-earth-based quasicrystals and their approximants. ESR is a powerful technique to probe the local electronic environment of diluted local moments. It accesses the low-frequency transverse magnetization fluctuations of the

conduction electrons in the presence of a static magnetic field [43].

The reported ESR spectra in Ref. [36] displays Dysonian line shapes, characteristic of localized moments embedded in a conduction electron sea, thus giving access to the non-trivial electronic properties of quasiperiodic systems. In particular, the linewidth is linked to the local moment relaxation rate, $1/T_1^i$, which is given by

$$\frac{1}{T_1^i T} \propto \lim_{\omega_0 \rightarrow 0} \frac{\chi''_{ii}(\omega_0)}{\omega_0} \propto \int d\omega \rho_i^2(\omega) \left(-\frac{\partial f}{\partial \omega} \right), \quad (5)$$

where $\chi''_{ii}(\omega_0)$ is the imaginary part of the dynamical susceptibility of the conduction electrons, ω_0 is the ESR resonance frequency, $\rho_i(\omega)$ is the local density of states, and f is the Fermi-Dirac distribution. In a regular metal, $\rho_i(\omega)$ is roughly constant around the Fermi level and we get a constant $1/T_1 T$ at low temperatures, a behavior known as Korringa relaxation law [73]. Given the complex nature of the electronic states in a quasicrystal, it is an interesting question to check if this law holds both in the approximant and in the thermodynamic limit of the quasicrystal because it is not obvious that one can neglect the generically strong fluctuations of $\rho_i(\omega)$ as a function of ω .

Modeling the conduction electrons with Eq. (1), we calculate the local relaxation in Eq. (5) rate using KPM since it gives us direct access to the local density of states. For diluted impurities, we do not select a local environment with a given z and compute $\langle 1/T_1 \rangle = N^{-1} \sum_{i=1}^N 1/T_1^i$ considering all sites in the approximant. We did check that the general conclusions we present hold for averages taken over a subset of sites with a given z , as expected by the inflation symmetry.

In Fig. 14(a) we show $\langle 1/T_1 T \rangle$ as a function of the temperature for the $N = 275807$ approximant. For all fillings considered, we recover the Korringa relaxation law at low temperatures, $T \lesssim 0.005t$. The fillings $n = 2/s^4$ and $n = 2/s^2$ correspond to pseudogaps in the density of states for $N \rightarrow \infty$. This amounts for the small values of $\langle 1/T_1 T \rangle$ for those two fillings in comparison to the more generic fillings $1/2$ and $7/8$. Actually, for $n = 2/s^2$, $\langle 1/T_1 T \rangle$ still shows a mild temperature dependence down to $T \rightarrow 0$.

Extrapolating the curves $\langle 1/T_1 T \rangle$ down to $T = 0$, we plot $\langle 1/T_1 T \rangle_{T \rightarrow 0} \times N$. We normalize $\langle 1/T_1 T \rangle_{T \rightarrow 0}$ by its value at $N = 239$ to account for the differences in scale coming from $\rho(\omega)$. The curves are well fitted by a power law, $\langle 1/T_1 T \rangle_{T \rightarrow 0} \sim N^{-\alpha}$. For the fillings $n = 2/s^4$ and $n = 2/s^2$, the decay is sharper because of the expected pseudogap in the thermodynamic limit. For $n = 7/8$, there is a milder decay, indicating that $\rho(\omega)$ is reduced with N for this particular filling. Interestingly, for $n = 1/2$ $\rho(\omega)$ increases and $\alpha < 0$. Since the integral of $\rho(\omega)$ over all states is 2, the decrease at a given filling must be compensated by an increase elsewhere. Most of this enhancement comes from $n = 1$ at $\omega = 0$ where the existence of localized states imply that $\rho(\omega \rightarrow 0) \rightarrow \infty$ for $N \rightarrow \infty$ [51].

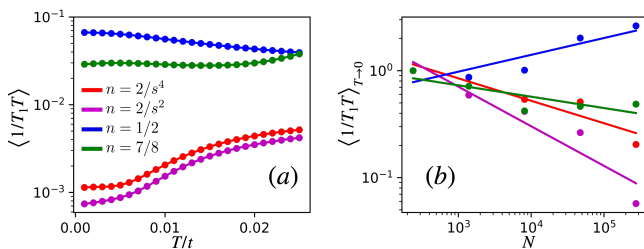


Figure 14. Average spin relaxation rate, $\langle 1/T_1 \rangle$, divided by T , in a metallic quasicrystal. (a) $\langle 1/T_1 T \rangle$ as a function of T for the approximant $N = 275807$ and several fillings n in a mono-log scale. (b) Scaling of $\langle 1/T_1 T \rangle$, in the limit $T \rightarrow 0$, as a function of the approximant size in a log-log scale. We normalize the relaxation rates for different N by their values for $N = 239$. We use the same color scheme as in (a) and fit the data by a power-law: $\langle 1/T_1 T \rangle_{T \rightarrow 0} \sim N^{-\alpha}$, $\alpha = 0.21$ (4), 0.37 (7), -0.16 (5), and 0.11 (4) for $n = 2/s^4$, $2/s^2$, $1/2$, and $7/8$, respectively.

Overall, a generic filling might increase or decrease the value of the relaxation rate as one approaches the thermodynamic limit. Such a finite-size study is not feasible in a periodic solid-state system. However, one can contrast the behavior of approximant and the thermodynamic quasicrystal in a quasiperiodic system, as one controls the size of the unit cell [36]. If these results are interpreted according to the general scenario suggested by Fig. 14, one might gain valuable information regarding the non-trivial electronic structure of quasicrystals.

VI. CONCLUSIONS

Motivated by experimental studies of magnetic order in rare-earth metallic quasicrystals [34, 36, 37], we followed Refs. [30, 31] and studied local Ising moments placed in the two-dimensional Ammann-Beenker and Penrose tiling. Modeling the electronic properties of this quasiperiodic system via a tight-binding model, we investigated the resulting ordering states for local moments interacting via a minimal set of RKKY-like interactions [41]. Taking advantage of the fact that in a quasicrystal we have different local environments, we place the local moments in a deterministic fashion: the spins occupy all sites with a given local coordination number z .

Monte Carlo simulations in finite tilings, combined with usual finite size scaling, show that the system generically develops long-range order at low temperatures [30, 31]. Therefore, the lack of periodicity and local moments interacting via RKKY couplings are insufficient to generate a spin-glass, and true randomness is required. This scenario is broadly consistent with the experimental results, for instance, in Refs. [34, 36, 37], reporting long-range order in rare-earth-based metallic quasicrystalline approximants. Our results suggest these magnetic states to be quite complex and fragile, owing to the presence of quasiperiodicity and frustration. In particular, a

fraction of the sites might fluctuate to low temperatures since they feel no mean field due to the ordered spins. One experimental signature of such a partially disordered state is a residual ground state entropy, which should be quenched in external fields.

Due to these disordered spin clusters, perturbations substantially impact the ordered state. In particular, we show that the introduction of vacancies turns this ordered state of the approximant into a spin-glass [37].

For the quasicrystal, one might envision the following situation. Consider a cluster of fluctuating spins of size D , which is weakly coupled to the ordered local moments. According to Conway's theorem [74], such a local pattern is never more than a distance $2D$ of a precisely identical region. This implies a finite fraction of spins experiencing weak mean fields from the ordered local moments in the limit $N \rightarrow \infty$. An extrinsic perturbation can thus easily pin these spins into random directions, effectively generating a random field on the ordered spins that will melt the long-range order [71, 72, 75]. Such a mechanism could help explain why experiments in magnetic quasicrystals generically identify spin-glass order.

The ESR experiments of Ref. [36] report that, in the diluted limit, the local moment relaxation rate $1/T_1 T$ obeys the Korringa relaxation law, both for the approximant and the quasicrystal. However, $1/T_1 T$ diminishes as one moves from the approximant to the quasicrystal. Within our simple model, one could interpret this result assuming that the Fermi level of the conduction electrons sits close to a pseudogap, as it is often the case with metallic quasicrystals [26–28]. However, further investigation is required, for instance, by performing transport [33, 76] and spectroscopy measurements [77].

In conclusion, we studied the behavior of local moments in contact with a quasiperiodic conduction electron bath. The spin-relaxation rate in the diluted limit depends on the system size N and the electronic filling n . If the Fermi energy sits at a pseudogap for $N \rightarrow \infty$, the relaxation rate is suppressed with system size. For a finite concentration of magnetic impurities, we investigated the resulting ordering pattern if these spins interact via RKKY-like interactions, mediated by the electronic bath. For impurities occupying all sites with a fixed number of nearest neighbors in the approximants, we generically find long-range magnetic order for finite N . However, the resulting magnetic state is generically fragile, usually displaying clusters of essentially free spins. As $N \rightarrow \infty$, these clusters become increasingly sensitive to extrinsic defects and could nucleate random fields destabilizing the long-range magnetic order, paving the way for a spin-glass state. Local probes investigating the local distribution of fields, like NMR, could be useful in testing this scenario.

ACKNOWLEDGMENTS

We acknowledge useful discussions with M. Ávila, V. Dobrosavljević, M. Cabrera-Baez, A. Jagannathan, and M. Vojta. We thank the anonymous referees for the insightful referring process that markedly improved our manuscript. R.N.A was supported by the CAPES (Brazil) - Finance Code 001. C.C.B was supported by FAPESP (Brazil), Grants No. 2022/14330-1 and 2023/06101-5. ECA was supported by CNPq (Brazil), Grant No. 302823/2022-0, and FAPESP (Brazil), Grants No. 2021/06629-4 and 2022/15453-0.

Appendix A: Further exchange couplings

We now present results including extra exchange couplings in Eq. (3). Specifically, we consider $J_{5(4)}$ between fifth (fourth) neighbor for impurities placed in the $z = 3(4)$ local environment of the octagonal tiling.

For $z = 3$, we consider $n = 2/s^2$ and the sample results are displayed in Fig. 15. Despite a ferromagnetic

J_5 , see Fig. 15(c), the critical temperature is reduced to $T_N = 0.505(5)J_1$, indicating an enhancement in frustration. However, the results are qualitatively similar, as shown by the residual entropy s_0 and the local exchange field distribution for $T < T_N$, Figs. 7(c) and 7(d). Because $P(h_i \rightarrow 0) \neq 0$ and s_0 hardly change, we conclude that longer-range couplings do not quench the fluctuating spin islands for $T \rightarrow 0$. This conclusion agrees with Refs. [30, 31]. These references report fluctuating spins even when taking into account exchange couplings between all spin pairs as determined by the full set of RKKY interactions.

For $z = 4$, we consider the filling $n = 7/8$ and a fourth neighbor exchange J_4 , see Fig. 16(d), which is again ferromagnetic. The critical temperature slightly increases to $T_N = 1.31(1)|J_1|$, but the results hardly change with respect to Fig. 10.

As longer-range couplings tend to diminish in magnitude, see Fig. 2, we conclude that further couples do not alter qualitatively the scenario presented in the main text. Therefore, keeping the minimal set of J_i 's is sufficient to capture the key aspects of the model.

-
- [1] D. Shechtman, I. Blech, D. Gratias, and J. W. Cahn, Metallic Phase with Long-Range Orientational Order and No Translational Symmetry, *Phys. Rev. Lett.* **53**, 1951 (1984).
- [2] T. Janssen, G. Chapuis, and M. de Boissieu, *Aperiodic Crystals: From Modulated Phases to Quasicrystals: Structure and Properties*, International Union of Crystallography Monographs on Crystallography (OUP Oxford, 2018).
- [3] S. J. Ahn, P. Moon, T.-H. Kim, H.-W. Kim, H.-C. Shin, E. H. Kim, H. W. Cha, S.-J. Kahng, P. Kim, M. Koshino, Y.-W. Son, C.-W. Yang, and J. R. Ahn, Dirac electrons in a dodecagonal graphene quasicrystal, *Science* **361**, 782 (2018).
- [4] W. Yao, E. Wang, C. Bao, Y. Zhang, K. Zhang, K. Bao, C. K. Chan, C. Chen, J. Avila, M. C. Asensio, J. Zhu, and S. Zhou, Quasicrystalline 300 twisted bilayer graphene as an incommensurate superlattice with strong interlayer coupling, *Proc. Natl. Acad. Sci. USA* **115**, 6928 (2018).
- [5] A. Uri, S. C. de la Barrera, M. T. Randeria, D. Rodan-Legrain, T. Devakul, P. J. D. Crowley, N. Paul, K. Watanabe, T. Taniguchi, R. Lifshitz, L. Fu, R. C. Ashoori, and P. Jarillo-Herrero, Superconductivity and strong interactions in a tunable moiréquasicrystal, *Nature* **620**, 762 (2023).
- [6] K. Viebahn, M. Sbroscia, E. Carter, J.-C. Yu, and U. Schneider, Matter-wave diffraction from a quasicrystalline optical lattice, *Phys. Rev. Lett.* **122**, 110404 (2019).
- [7] S. N. Kempkes, M. R. Slot, S. E. Freaney, S. J. M. Zevenhuizen, D. Vanmaekelbergh, I. Swart, and C. M. Smith, Design and characterization of electrons in a fractal geometry, *Nat. Phys.* **15**, 127 (2019).
- [8] H. Huang and F. Liu, Quantum spin hall effect and spin bott index in a quasicrystal lattice, *Phys. Rev. Lett.* **121**, 126401 (2018).
- [9] R. Ghadimi, T. Sugimoto, K. Tanaka, and T. Tohyama, Topological superconductivity in quasicrystals, *Phys. Rev. B* **104**, 144511 (2021).
- [10] A. Grossi e Fonseca, T. Christensen, J. D. Joannopoulos, and M. Soljačić, Quasicrystalline weyl points and dense fermi-bragg arcs, *Phys. Rev. B* **108**, L121109 (2023).
- [11] K. Deguchi, S. Matsukawa, N. K. Sato, T. Hattori, K. Ishida, H. Takakura, and T. Ishimasa, Quantum critical state in a magnetic quasicrystal, *Nat. Mater.* **11**, 1013 (2012).
- [12] S. Takemura, N. Takemori, and A. Koga, Valence fluctuations and electric reconstruction in the extended Anderson model on the two-dimensional Penrose lattice, *Phys. Rev. B* **91**, 165114 (2015).
- [13] E. C. Andrade, A. Jagannathan, E. Miranda, M. Vojta, and V. Dobrosavljević, Non-Fermi-Liquid Behavior in Metallic Quasicrystals with Local Magnetic Moments, *Phys. Rev. Lett.* **115**, 036403 (2015).
- [14] N. Hartman, W.-T. Chiu, and R. T. Scalettar, Magnetic correlations in a periodic Anderson model with nonuniform conduction electron coordination, *Phys. Rev. B* **93**, 235143 (2016).
- [15] A. Koga and H. Tsunetsugu, Antiferromagnetic order in the Hubbard model on the Penrose lattice, *Phys. Rev. B* **96**, 214402 (2017).
- [16] S. Sakai, N. Takemori, A. Koga, and R. Arita, Superconductivity on a quasiperiodic lattice: Extended-to-localized crossover of Cooper pairs, *Phys. Rev. B* **95**, 024509 (2017).
- [17] K. Kamiya, T. Takeuchi, N. Kabeya, N. Wada, T. Ishimasa, A. Ochiai, K. Deguchi, K. Imura, and N. K. Sato, Discovery of superconductivity in quasicrystal, *Nat. Commun.* **9**, 154 (2018).
- [18] R. N. Araújo and E. C. Andrade, Conventional super-

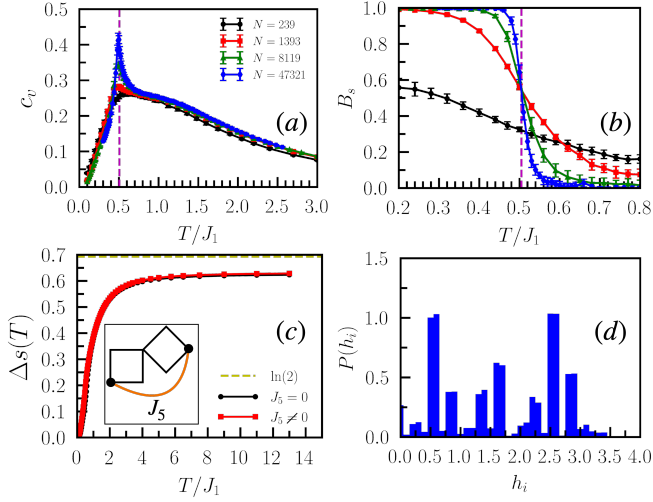


Figure 15. Characterization of the ordered states for local moments placed at the $z = 3$ sites of the Ammann-Beenker tiling for $n = 2/s^2$ and an extra coupling $J_5 = -0.142J_1$, see the inset of (c). (a) Specific heat as a function of the temperature T for several approximant sizes N . The vertical dashed line marks the position of the ordering temperature T_N . (b) Binder cumulant B_s of the order parameter as a function of T . The dashed line marks the crossing of the curves for $N \geq 1393$ and determines $T_N = 0.505(5)J_1$. The curve colors are the same as in (a). (c) Residual entropy $\Delta s(T)$, per site, as a function of T for $N = 8119$. The dashed line gives $s(T \rightarrow \infty) = \log 2$. (d) Histogram of the local exchange field, $P(h_i)$, for $T < T_N$.

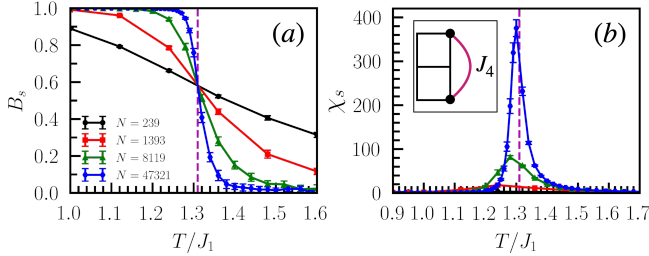


Figure 16. Characterization of the ordered states for local moments placed at the $z = 4$ sites, $n = 7/8$ and an extra coupling $J_4 = -0.077|J_1|$, see the inset of (b). (a) Binder cumulant B_s of the order parameter as a function of T . The dashed line marks the crossing of the curves and determines $T_N = 1.31(1)|J_1|$. (b) Order parameter susceptibility χ_s as a function of T . The vertical dashed line marks the position of the ordering temperature T_N . The curve colors are the same as in (a).

conductivity in quasicrystals, *Phys. Rev. B* **100**, 014510 (2019).

- [19] S. Sakai and R. Arita, Exotic pairing state in quasicrystalline superconductors under a magnetic field, *Phys. Rev. Res.* **1**, 022002 (2019).
- [20] G. Rai, S. Haas, and A. Jagannathan, Superconducting proximity effect and order parameter fluctuations in disordered and quasiperiodic systems, *Phys. Rev. B* **102**,

134211 (2020).

- [21] Y. Cao, Y. Zhang, Y.-B. Liu, C.-C. Liu, W.-Q. Chen, and F. Yang, Kohn-luttinger mechanism driven exotic topological superconductivity on the penrose lattice, *Phys. Rev. Lett.* **125**, 017002 (2020).
- [22] P. Fazekas, *Lecture Notes on Electron Correlation and Magnetism*, EBL-Schweitzer (World Scientific, 1999).
- [23] K. Fischer and J. Hertz, *Spin Glasses*, Cambridge Studies in Magnetism (Cambridge University Press, 1993).
- [24] M. Kohmoto and B. Sutherland, Electronic States on a Penrose Lattice, *Phys. Rev. Lett.* **56**, 2740 (1986).
- [25] M. Arai, T. Tokihiro, T. Fujiwara, and M. Kohmoto, Strictly localized states on a two-dimensional Penrose lattice, *Phys. Rev. B* **38**, 1621 (1988).
- [26] T. Fujiwara, Electronic structure in the Al-Mn alloy crystalline analog of quasicrystals, *Phys. Rev. B* **40**, 942 (1989).
- [27] T. Fujiwara and T. Yokokawa, Universal pseudogap at Fermi energy in quasicrystals, *Phys. Rev. Lett.* **66**, 333 (1991).
- [28] S. Jazbec, S. Vrtnik, Z. Jagličić, S. Kashimoto, J. Ivkov, P. Popčević, A. Smontara, H. J. Kim, J. G. Kim, and J. Dolinšek, Electronic density of states and metastability of icosahedral Au-Al-Yb quasicrystal, *J. Alloys Compd.* **586**, 343 (2014).
- [29] A. Jagannathan, The fibonacci quasicrystal: Case study of hidden dimensions and multifractality, *Rev. Mod. Phys.* **93**, 045001 (2021).
- [30] S. Thiem and J. T. Chalker, Magnetism in rare-earth quasicrystals: RKKY interactions and ordering, *Europhys. Lett.* **110**, 17002 (2015).
- [31] S. Thiem and J. T. Chalker, Long-range magnetic order in models for rare-earth quasicrystals, *Phys. Rev. B* **92**, 224409 (2015).
- [32] H. Miyazaki, T. Sugimoto, K. Morita, and T. Tohyama, Magnetic orders induced by rkkY interaction in tsai-type quasicrystalline approximant au-al-gd, *Phys. Rev. Mater.* **4**, 024417 (2020).
- [33] I. R. Fisher, K. O. Cheon, A. F. Panchula, P. C. Canfield, M. Chernikov, H. R. Ott, and K. Dennis, Magnetic and transport properties of single-grain $R - Mg - Zn$ icosahedral quasicrystals [$R = Y, (Y_{1-x}Gd_x), (Y_{1-x}Tb_x), Tb, Dy, Ho, \text{ and } Er$], *Phys. Rev. B* **59**, 308 (1999).
- [34] A. I. Goldman, T. Kong, A. Kreyssig, A. Jesche, M. Ramazanoglu, K. W. Dennis, S. L. Bud'ko, and P. C. Canfield, A family of binary magnetic icosahedral quasicrystals based on rare earths and cadmium, *Nat. Mater.* **12**, 714 (2013).
- [35] T. Kong, S. L. Bud'ko, A. Jesche, J. McArthur, A. Kreyssig, A. I. Goldman, and P. C. Canfield, Magnetic and transport properties of $i-r$ -cd icosahedral quasicrystals ($r = Y, Gd-Tm$), *Phys. Rev. B* **90**, 014424 (2014).
- [36] M. Cabrera-Baez, M. A. Avila, and C. Rettori, Conduction electrons in aperiodic versus periodic structures: An esr study of quasicrystalline $i-y(gd)$ -cd and its approximant $Y(Gd)cd_6$, *Phys. Rev. B* **100**, 014207 (2019).
- [37] T. Shiino, F. Denoel, G. H. Gebresenbut, D. C. Joshi, Y.-C. Huang, C. P. Gómez, U. Häussermann, A. Rydh, and R. Mathieu, Singular magnetic dilution behavior in a quasicrystal approximant, *Phys. Rev. B* **104**, 224411 (2021).
- [38] J. E. S. Socolar, Simple octagonal and dodecagonal quasicrystals, *Phys. Rev. B* **39**, 10519 (1989).
- [39] A. Jagannathan and F. Piéchon, Energy levels and

- their correlations in quasicrystals, *Philos. Mag.* **87**, 2389 (2007).
- [40] M. Duneau, R. Mosseri, and C. Oguey, Approximants of quasiperiodic structures generated by the inflation mapping, *J. Phys. A: Math. Gen.* **22**, 4549 (1989).
- [41] M. Duneau, F. Dunlop, A. Jagannathan, and C. Oguey, Frustrated ising models on quasiperiodic lattices in two dimensions, *Mod. Phys. Lett. B* **05**, 1895 (1991).
- [42] A. Weiße, G. Wellein, A. Alvermann, and H. Fehske, The kernel polynomial method, *Rev. Mod. Phys.* **78**, 275 (2006).
- [43] S. Barnes, Theory of electron spin resonance of magnetic ions in metals, *Adv. Phys.* **30**, 801 (1981).
- [44] E. S. Sørensen, M. V. Jarić, and M. Ronchetti, Ising model on penrose lattices: Boundary conditions, *Phys. Rev. B* **44**, 9271 (1991).
- [45] D. Ledue, D. P. Landau, and J. Teillet, Static critical behavior of the ferromagnetic ising model on the quasiperiodic octagonal tiling, *Phys. Rev. B* **51**, 12523 (1995).
- [46] A. Jagannathan and M. Duneau, Properties of the ammann-beenker tiling and its square periodic approximants, *Isr. J. Chem.* **n/a**, e202300119.
- [47] H. Lee, J. Kim, E. R. Mucciolo, G. Bouzerar, and S. Kettemann, Rkky interaction in disordered graphene, *Phys. Rev. B* **85**, 075420 (2012).
- [48] J. H. García, L. Covaci, and T. G. Rappoport, Real-space calculation of the conductivity tensor for disordered topological matter, *Phys. Rev. Lett.* **114**, 116602 (2015).
- [49] M. G. Yamada, Anderson–Kitaev spin liquid, *npj Quantum Materials* **5**, 82 (2020).
- [50] A.-K. Wu, D. Bauernfeind, X. Cao, S. Gopalakrishnan, K. Ingersent, and J. H. Pixley, Aubry–andré anderson model: Magnetic impurities coupled to a fractal spectrum, *Phys. Rev. B* **106**, 165123 (2022).
- [51] T. Rieth and M. Schreiber, Identification of spatially confined states in two-dimensional quasiperiodic lattices, *Phys. Rev. B* **51**, 15827 (1995).
- [52] J. Jeon and S. Lee, Anomalous long-distance rkky interaction in quasicrystals (2023), [arXiv:2310.15228 \[cond-mat.str-el\]](https://arxiv.org/abs/2310.15228).
- [53] K. Hukushima and K. Nemoto, Exchange monte carlo method and application to spin glass simulations, *J. Phys. Soc. Jpn.* **65**, 1604 (1996).
- [54] M. Newman and G. Barkema, *Monte Carlo Methods in Statistical Physics* (Clarendon Press, 1999).
- [55] K. Binder and A. P. Young, Spin glasses: Experimental facts, theoretical concepts, and open questions, *Rev. Mod. Phys.* **58**, 801 (1986).
- [56] P. Repetowicz, U. Grimm, and M. Schreiber, High-temperature expansion for ising models on quasiperiodic tilings, *J. Phys. A: Math. Gen.* **32**, 4397 (1999).
- [57] S. Wessel, A. Jagannathan, and S. Haas, Quantum Antiferromagnetism in Quasicrystals, *Phys. Rev. Lett.* **90**, 177205 (2003).
- [58] J. M. Luck, A Classification of Critical Phenomena on Quasi-Crystals and Other Aperiodic Structures, *Europhys. Lett.* **24**, 359 (1993).
- [59] M. Gallone and V. Mastropietro, [Universality in the 2d quasi-periodic ising model and harris-luck irrelevance](https://arxiv.org/abs/2304.01736) (2024), [arXiv:2304.01736 \[math-ph\]](https://arxiv.org/abs/2304.01736).
- [60] C. Santamaria and H. T. Diep, Evidence of partial disorder in a frustrated Heisenberg spin system, *J. Appl. Phys.* **81**, 5276 (1997).
- [61] A. S. Wills, R. Ballou, and C. Lacroix, Model of localized highly frustrated ferromagnetism: The kagome spin ice, *Phys. Rev. B* **66**, 144407 (2002).
- [62] B. Javanparast, Z. Hao, M. Enjalran, and M. J. P. Gingras, Fluctuation-driven selection at criticality in a frustrated magnetic system: The case of multiple- \mathbf{k} partial order on the pyrochlore lattice, *Phys. Rev. Lett.* **114**, 130601 (2015).
- [63] M. G. Gonzalez, F. T. Lisandrini, G. G. Blesio, A. E. Trumper, C. J. Gazza, and L. O. Manuel, Correlated partial disorder in a weakly frustrated quantum antiferromagnet, *Phys. Rev. Lett.* **122**, 017201 (2019).
- [64] U. F. P. Seifert and M. Vojta, Theory of partial quantum disorder in the stuffed honeycomb Heisenberg antiferromagnet, *Phys. Rev. B* **99**, 155156 (2019).
- [65] E. C. Andrade and M. Vojta, Partial magnetic order in kagome spin ice, *Phys. Rev. B* **109**, L241102 (2024).
- [66] R. Ghadimi, T. Sugimoto, and T. Tohyama, Mean-field study of the bose-hubbard model in the penrose lattice, *Phys. Rev. B* **102**, 224201 (2020).
- [67] A. P. Young, Direct determination of the probability distribution for the spin-glass order parameter, *Phys. Rev. Lett.* **51**, 1206 (1983).
- [68] A. J. Bray and M. A. Moore, Lower critical dimension of ising spin glasses: a numerical study, *J. Phys. C: Solid State Phys* **17**, L463 (1984).
- [69] J. Colbois, B. Vanhecke, L. Vanderstraeten, A. Smerald, F. Verstraete, and F. Mila, Partial lifting of degeneracy in the $J_1-J_2-J_3$ Ising antiferromagnet on the kagome lattice, *Phys. Rev. B* **106**, 174403 (2022).
- [70] M. R. Cantarino, R. P. Amaral, R. S. Freitas, J. C. R. Araújo, R. Lora-Serrano, H. Luetkens, C. Baines, S. Bräuninger, V. Grinenko, R. Sarkar, H. H. Klauss, E. C. Andrade, and F. A. Garcia, Dynamic magnetism in the disordered hexagonal double perovskite $\text{BaTi}_{1/2}\text{Mn}_{1/2}\text{O}_3$, *Phys. Rev. B* **99**, 054412 (2019).
- [71] M. M. J. Miranda, I. C. Almeida, E. C. Andrade, and J. A. Hoyos, Phase diagram of a frustrated heisenberg model: From disorder to order and back again, *Phys. Rev. B* **104**, 054201 (2021).
- [72] X. Ye, R. Narayanan, and T. Vojta, Stripe order, impurities, and symmetry breaking in a diluted frustrated magnet, *Phys. Rev. B* **105**, 024201 (2022).
- [73] P. Coleman, *Introduction to Many-Body Physics* (Cambridge University Press, 2015).
- [74] M. Gardner, Extraordinary nonperiodic tiling that enriches the theory of tiles, *Sci. Amer.* **236**, 110 (1977).
- [75] A. Aharony, Absence of Ferromagnetic Long Range Order in Random Isotropic Dipolar Magnets and in similar systems, *Solid State Commun.* **28**, 667 (1978).
- [76] F. S. Pierce, S. J. Poon, and Q. Guo, Electron Localization in Metallic Quasicrystals, *Science* **261**, 737 (1993).
- [77] V. A. Rogalev, O. Gröning, R. Widmer, J. H. Dil, F. Bisti, L. L. Lev, T. Schmitt, and V. N. Strocov, Fermi states and anisotropy of Brillouin zone scattering in the decagonal Al-Ni-Co quasicrystal, *Nat. Commun.* **6**, 8607 (2015).